Inorganica Chimica Acta 366 (2011) 203–208

Contents lists available at ScienceDirect

Inorganica Chimica Acta

journal homepage: www.elsevier.com/locate/ica

New chelate complexes of trivalent Y and lanthanides (Eu, Ho, Yb) with a triazene N-oxide: Synthesis, structural characterization and luminescence properties

Gelson Manzoni de Oliveira [a,*], Manfredo Hörner [a,*], Aline Machado [a], Davi F. Back [a], Jorge H.S.K. Monteiro [b], Marian R. Davolos [b]

[a] Universidade Federal de Santa Maria, UFSM, Departamento de Química, 97105-900 Santa Maria, RS, Brazil
[b] Universidade Estadual Paulista, UNESP, Instituto de Química, Laboratório de Materiais Luminescentes, Rua Francisco Degni s/n, 14800-900 Araraquara, SP, Brazil

ARTICLE INFO

Article history:
Received 1 July 2010
Received in revised form 25 October 2010
Accepted 3 November 2010
Available online 12 November 2010

Dedicated to the memory of Professor Herbert Schumann

Keywords:
Lanthanides(III) chelate complexes
Triazene oxides complexes of lanthanides
Luminescence of lanthanides(III) complexes

ABSTRACT

Deprotonated 3-(4-nitrophenyl)-1-phenyltriazene N-oxide reacts with $YCl_3{\cdot}6H_2O$ and $LnCl_3{\cdot}6H_2O$ (Ln = Eu, Ho, Yb) to give the monoclinic chelate complexes $[Y\{O_2N(C_6H_4)NNN(O)Ph\}_4](Et_3NH){\cdot}H_2O$ (**1**) (Ph = C_6H_5; Et = C_2H_5) and $[Ln^{III}\{O_2N(C_6H_4)NNN(O)Ph\}_4](Et_3NH){\cdot}H_2O{\cdot}\{CH_3OH^*\}$ {Ln^{III} = Eu (**2**), Ho (**3**), Yb* (**4**), in which the metal centers present a square antiprismatic configuration. As already observed for hydrated ammonium complexes of triazene-oxides ligands with $(C_6H_4)-NO_2$ groups, multiple, effective O···H and N···H interactions hold the species in supramolecular 3D assemblies. The optical and the luminescent properties of the triazene-oxide europium complex **2** are also presented and fully discussed.

1. Introduction

Triazenes present a remarkable ability to perform variable coordination modes with transition metals, showing also a noteworthy trend to achieve intermolecular, secondary metal–ligand and ligand–ligand interactions. Such characteristics make these species also proficient to assemble unique supramolecular aggregates. Recently we have reported some examples of these classes of compounds, with 1D [1–4] and 2D [5–7] polymeric assemblies. The generation "in situ" of an alkali metal derivative was also investigated, by reaction of the relatively unstable 3-(4-carboxyphenyl)-1-methyltriazene N-oxide with KOH [8].

The early reported species called triazenes 1-oxides [9] present a hydroxyl group in the N1-atom of the triazene chain and result from the equilibrium shown in the Scheme 1.

In solution, triazenes oxides appear in the form **I**, while the tautomeric form **II** is preferred in the solid state (powder or crystalline). Because of the hard (medium) basic character of the O (N) atoms, associated with the negative charge of the deprotonated form, and the proximity of the two coordinative sites (O and N), triazenes oxides are in general good chelators, with a noteworthy tendency to achieve stable five-membered rings (**A**) with transition metal ions [10,11].

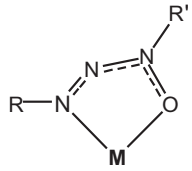

A

Due to the strong hydration of lanthanide salts, their complexation (chelation) is only achieved with stereochemically appropriated chelators, like, for example, the triazene oxide 3-(4-nitrophenyl)-1-phenyltriazene N-oxide. This species presents a relatively simple architecture, allied with the nearness of the coordinative sites and with the hard basic character of the O^- ligand, in this case an indispensable requisite for the displacement of the strong coordinated water molecules of the lanthanide salts. These theoretical predictions have been already demonstrated with the synthesis of the chelate complexes $[Ln^{III}\{O_2N(C_6H_4)NNN(O)Ph\}_4](Et_3NH){\cdot}H_2O$ ($M = La^{3+}$, Dy^{3+}; Ph = C_6H_5; Et = C_2H_5) [12]. Although known as good chelating agents for some lanthanides, so far triazenes have never been outstanding by their fluorescent

* Corresponding authors. Tel.: +55 55 3220 8757; fax: +55 55 3220 8031.
E-mail addresses: manzonideo@smail.ufsm.br (G. Manzoni de Oliveira), hoerner.manfredo@gmail.com (M. Hörner).

0020-1693/$ - see front matter © 2010 Elsevier B.V. All rights reserved.
doi:10.1016/j.ica.2010.11.007

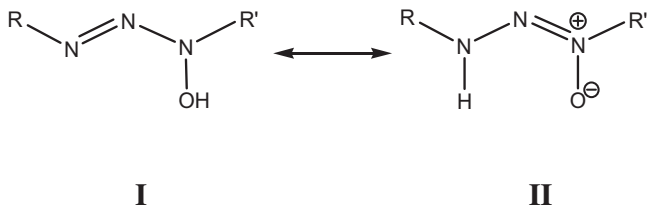

I II

Scheme 1. Tautomeric equilibrium of triazenes 1-oxides.

activities, still less by their ability to transfer energy to a lanthanide ion and so excite its luminescence.

The rare-earth elements are characterized for showing the electronic configuration [Xe] $4f^n$ ($n = 0$–14). The outer lying $5s^25p^6$ filled subshells of these elements are not luminescent, but the core electrons 4f show high luminescence activity due to intraconfigurational transitions 4f–4f, which are not allowed by Laporte and spin rules. Because of the effective shielding of the 4f orbitals and selection rules restrictions, the lanthanide transitions are little affected by the crystalline field and are narrow bands. The low crystalline field influence makes the lanthanides very good structural probes, especially Eu^{3+} [13] that shows the characteristic transitions $^5D_0 \rightarrow {}^7F_J$ ($J = 0$, 1, 2, 3 and 4), all in the red region, which depend on the number of nonsymmetrical sites ($^5D_0 \rightarrow {}^7F_0$), environment ($^5D_0 \rightarrow {}^7F_2$) and long range effects ($^5D_0 \rightarrow {}^7F_4$). The narrow bands are very interesting and useful in processes requesting high efficiency and monochromaticity. The most exploited rare-earths are Sm^{3+}, with emission in the orange region, Eu^{3+} (red emission) [14], and Tb^{3+} with green emission. The theoretical tools provide a good deal of informations about various and important features, like, for example, coordination polyhedrons and triplet/singlet states energies.

We report now some further results on the complex structural chemistry of triazenes and lanthanides together with luminescence studies carried out with the new chelates $[Y^{III}\{O_2N(C_6H_4)NNN(O)Ph\}_4](Et_3NH)\cdot H_2O$ (**1**) and $[Ln^{III}\{O_2N(C_6H_4)NNN(O)Ph\}_4](Et_3NH)\cdot H_2O\cdot\{CH_3OH^*\}$ {Ln^{III} = Eu (**2**), Ho (**3**), Yb* (**4**)}, obtained by deprotonation of 3-(4-nitrophenyl)-1-phenyltriazene N-oxide with triethylamine and further reaction with $YCl_3\cdot 6H_2O$/$LnCl_3\cdot 6H_2O$. We demonstrate also the worth of theoretical methods associated with the characteristic transitions of the Eu^{3+} luminescence to help the crystallographic structural studies and to explain the low luminescence of the parent complexes. Since the optical and structural properties of the "semi" lanthanide yttrium arouse increasing interest, results regarding its triazene complex have been also included in this work.

2. Experimental

2.1. General

Elemental analyses for C, H and N were performed at a Shimadzu EA 112 microanalysis instrument. IR spectra were recorded on a Tensor 27 – Bruker spectrometer with KBr pellets in the 4000–400 cm^{-1} region. Methanol was dried with Mg/I_2 and distilled prior to use. The complex $[Gd\{O_2NPhNNN(O)Ph\}_4](Et_3NH)\cdot H_2O$, employed for determination of the triplet energy level of the ligand, was prepared according the standard procedure used in this work and identified with basis on elemental analysis and IR spectra.

2.2. Synthesis of $[Y\{O_2N(C_6H_4)NNN(O)Ph\}_4](Et_3NH)\cdot H_2O$ (1) and $[Ln\{O_2N(C_6H_4)NNN(O)Ph\}_4](Et_3NH)\cdot H_2O\cdot\{CH_3OH^*\}$ {Ln^{III} = Eu (2), Ho (3), Yb* (4)}

The ligand 3-(4-nitrophenyl)-1-phenyltriazene N-oxide (0.0514 g, 0.2 mmol) was dissolved in 10 mL of anhydrous methanol at 65 °C. Small portions of $YCl_3\cdot 6H_2O$ (0.0152 g, 0.05 mmol), or $LnCl_3\cdot 6H_2O$ {0.05 mmol: 0.0183 g (**2**); 0.01896 g (**3**); 0.0194 g (**4**)} were added under continuous stirring to the yellow solution. After addition of five drops of triethylamine the color of the solution turned dark-purple. The mixture was refluxed slowly under stirring for 2 h and then filtered for isolation of a deep-red precipitate. The slow evaporation of the solvent at room temperature yielded red crystals of **1**–**4**. Yields: 88% (**1**); 81% (**2**); 89% (**3**); 79% (**4**).

*Complex **1***: Melting point: 174 °C. *Anal.* Calc. for $C_{54}H_{54}YN_{17}O_{13}$: C, 52.39; H, 4.40; N, 19.23. Found: C, 48.34; H, 3.91; N, 17.67%. IR spectra (KBr): 3416 [strong, ν_s(N–H)]; 1659 [medium, ν_s(C=C)]; 1311 [strong, $\nu_s(NO_2)$]; 1401 [strong, ν_{as}(NNN)]; 1237 [strong, ν_s(N–O)]; 1105 cm^{-1} [medium, ν_s(N–N)].

*Complex **2***: Melting point: 193 °C. *Anal.* Calc. for $C_{54}H_{54}EuN_{17}O_{13}$: C, 49.85; H, 4.18; N, 18.30. Found: C, 49.22; H, 3.73; N, 17.92%. IR spectra (KBr): 3074 [s, ν_s(N–H)]; 1585 [m, ν_s(C=C)]; 1398 [s, $\nu_s(NO_2)$]; 1329 [s, ν_{as}(NNN)]; 1236 [s, ν_s(N–O)]; 1174 cm^{-1} [m, ν_s(N–N)].

*Complex **3***: Melting point: 197 °C. *Anal.* Calc. for $C_{54}H_{54}HoN_{17}O_{13}$: C, 49.36; H, 4.14; N, 18.12. Found: C, 49.22; H, 3.73; N, 17.92%. IR spectra (KBr): 3190 [s, ν_s(N–H)]; 1602 [m, ν_s(C=C)]; 1336 [s, $\nu_s(NO_2)$]; 1325 [s, ν_{as}(NNN)]; 1222 [s, ν_s(N–O)]; 1110 cm^{-1} [m, ν_s(N–N)].

*Complex **4***: Melting point: 196 °C. *Anal.* Calc. for $C_{55}H_{58}YbN_{17}O_{14}$: C, 47.75; H, 4.30; N, 17.53. Found: C, 49.22; H, 3.73; N, 17.92%. IR spectra (KBr): 3106 [s, ν_s(N–H)]; 1653 [m, ν_s(C=C)]; 1331 [s, $\nu_s(NO_2)$]; 1311 [s, ν_{as}(NNN)]; 1237 [s, ν_s(N–O)]; 1173 cm^{-1} [m, ν_s(N–N)].

2.3. X-ray crystallography

Data were collected with a Bruker APEX II CCD area-detector diffractometer and graphite-monochromatized Mo Kα radiation. The structures were solved by direct methods using SHELXS [15]. Subsequent Fourier-difference map analyses yielded the positions of the non-hydrogen atoms. Refinements were carried out with the SHELXL package [15]. All refinements were made by full-matrix least-squares on F^2 with anisotropic displacement parameters for all non-hydrogen atoms. Hydrogen atoms were included in the refinement in calculated positions.

2.4. Optical and luminescence experiments

For optimization of the ligand ground state geometry the RM1 model was used [16], implemented in MOPAC2009 package [17]. The optimization of the complex ground state geometry was carried out with the Sparkle/AM1 model [18] looking for a good result and low CPU time. Singlet and triplet states energies were calculated with the INDO/S-CIS [19,20] implemented in zindo package [21].

The ligand absorption spectrum in UV–Vis region was performed using dimethylsulfoxide (DMSO) as solvent in the Lambda 14P Perkin–Elmer equipment. The emission spectra of the complexes were recorded at ~77 K in a Spectrofluorimeter Fluorolog Horiba Jobin Yvon FL3-222 model with a 450 W Xenon lamp.

3. Results and discussion

3.1. Crystal structure

The X-ray crystal data and the experimental conditions for the analyses of $[Y^{III}\{O_2N(C_6H_4)NNN(O)Ph\}_4](Et_3NH)\cdot H_2O$ (**1**) and $[Ln^{III}\{O_2N(C_6H_4)NNN(O)Ph\}_4](Et_3NH)\cdot H_2O\cdot\{CH_3OH^*\}$ {Ln^{III} = Eu (**2**), Ho (**3**), Yb* (**4**)}, are given in Table 1. Table 2 resumes selected bond distances for the title complexes with basis on the templates of

Figs. 1 and 2 (structure of **2**), and Table 3 summarizes the most important bond angles of complex **2**. Fig. 1 shows the whole molecular structure (asymmetric unit) of **2**, with exception of the triethylammonium (counter) ion and the H_2O solvate molecule (the hydrogen atoms were also omitted by clarity). Fig. 2 displays the core of the anionic component of all complexes, with atom labeling for complex **2**.

In all the anionic species $[M\{O_2N(C_6H_4)NNN(O)Ph\}_4]^-$ (M = Y, Eu, Ho, Yb), represented for the Eu complex in Fig. 2, the metal centers present coordination number 8, with square antiprismatic geometry. The respectively four M–O and M–N bonds present different lengths, and the average distances are: Y–O = 2.2842/Y–N = 2.5447 (**1**); Eu–O = 2.3337/Eu–N = 2.5895 (**2**); Ho–O = 2.2822/Ho–N = 2.5402 (**3**); Yb–O = 2.2445/Yb–N = 2.5115 Å (**4**). The title compounds do not differ from analoge triazene complexes with respect to the ability of attaining intra and intermolecular secondary bonds, hence achieving polydimensional molecular aggregates. The counter ions Et_3NH^+ and the H_2O (solvate) molecules, allied to the presence of the NO_2 groups of the ligands, supply the conditions for the achievement of effective O···H and N···H interactions, which hold the molecules of the four $P2_1/c$-type products in three-dimensional, supramolecular assemblies. These interactions are already numerous even at relatively low adjustment of the connectivity (2.5 Å) between the atoms O/H and N/H in the bonds delimiter program [15] (the sum of the H–O/H–N van der Waals radii are 2.61 and 2.64 Å [22], respectively). As we have already shown in previous reports (see Introduction), the oxygen atoms of the N–(C_6H_4)–NO_2 ligand group are the main promoters of the O···H interactions, although the four metal-bonded oxygens also attain intramolecular bridges with vicinal phenyl hydrogen atoms, with variable distances. All compounds show intramolecular O···H bonds between the two oxygen atoms of all the (C_6H_4)–NO_2 groups with their own phenyl rings. In the crystal lattice of the title compounds the counter ions Et_3NH^+ and the solvate molecules (H_2O) are paired of through hydrogen bridges of the type NH···HOH . The N–H bond in the cation Et_3NH^+ measures 0.910 Å in all compounds. The single ligand 3-(4-nitrophenyl)-1-phenyltriazene N-oxide shows a strong infrared band at 3448.7 cm^{-1} [ν(O–H)], characteristic for the triazenes oxides. This band does not appear in the IR spectra of the products, since full deprotonation of the ligands occurs.

Table 2
Selected bond lengths [Å] for **1**, **2**, **3** and **4**.

	1	2	3	4
	Y	Eu	Ho	Yb
M–O1	2.270(2)	2.322(4)	2.267(6)	2.235(4)
M–O2	2.281(2)	2.333(4)	2.277(5)	2.247(4)
M–O3	2.289(2)	2.335(4)	2.289(5)	2.247(4)
M–O4	2.297(2)	2.345(4)	2.296(6)	2.249(4)
M–N43	2.516(3)	2.561(5)	2.506(7)	2.471(4)
M–N23	2.539(3)	2.585(5)	2.536(7)	2.515(5)
M–N33	2.552(3)	2.604(5)	2.551(7)	2.517(5)
M–N13	2.572(3)	2.608(5)	2.568(7)	2.543(4)

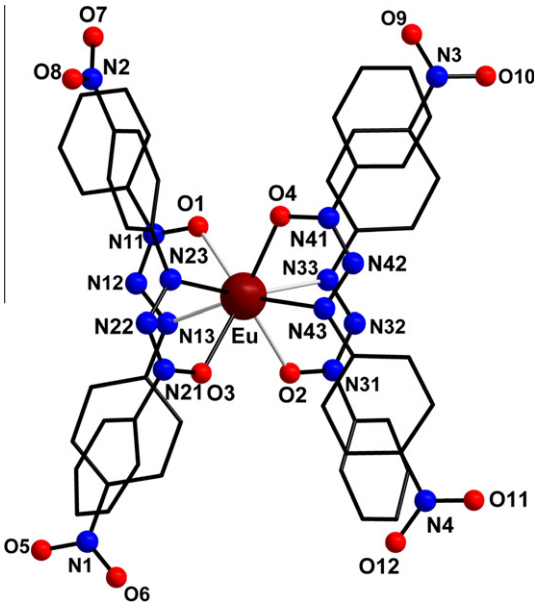

Fig. 1. Molecular structure of the complex anion $[Eu\{O_2N(C_6H_4)NNN(O)Ph\}_4]^-$ (**2**). For clarity, the counter ion $[Et_3NH]^+$, the solvate molecule (H_2O) and the hydrogen atoms are not shown.

Table 1
Crystal data and structure refinement for **1**···**4**.

	1	2	3	4
Empirical formula	$C_{54}H_{54}N_{17}O_{13}Y$	$C_{54}H_{54}N_{17}O_{13}Eu$	$C_{54}H_{54}N_{17}O_{13}Ho$	$C_{55}H_{58}N_{17}O_{14}Yb$
Formula weight	1238.05	1301.1	1314.07	1354.22
T (K)	140(2)	293(2)	293(2)	293(2)
Crystal system	monoclinic	monoclinic	monoclinic	monoclinic
Space group	$P2_1/c$	$P2_1/c$	$P2_1/c$	$P2_1/c$
a (Å)	9.0240(8)	9.0591(8)	9.1328(2)	9.1847(8)
b (Å)	20.1343(16)	20.2016(13)	20.3452(5)	19.8866(17)
c (Å)	31.055(3)	30.952(2)	31.1295(7)	32.237(3)
a (°)	90	90	90	90
b (°)	90.161(5)	90.323(3)	91.2360(10)	96.562(4)
g (°)	90	90	90	90
V (Å^3)	5642.4(9)	5664.4(7)	5782.8(2)	5849.6(9)
Z	4	4	4	4
ρ_{calc} (g cm^{-3})	1.457	1.526	1.509	1.538
μ (Mo Kα) (mm^{-1})	1.114	1.187	1.446	1.679
λ (Å)	0.71073	0.71073	0.71073	0.71073
F (0 0 0)	2560	2656	2672	2756
Collected reflections	46116	45783	52614	45743
Unique reflections	11908	12489	12807	11607
GOF (F^2)	0.968	1.133	0.963	0.947
R_1[a]	0.0539	0.054	0.0535	0.0421
wR_2[b]	0.1139	0.1427	0.17	0.1185

[a] $R_1 = ||F_o| - |F_c||/|F_o|$.
[b] $wR_2 = \{\sum w(F_o^2 - F_c^2)^2/\Sigma w(F_o^2)^2\}^{1/2}$.

Table 3
Selected bond angles for **2**.

O1–Eu–O2	127.56(15)	N43–Eu–N23	95.12(16)
O1–Eu–O3	125.37(15)	O1–Eu–N33	87.64(16)
O2–Eu–O3	75.21(15)	O2–Eu–N33	60.91(15)
O1–Eu–O4	78.86(14)	O3–Eu–N33	135.92(15)
O2–Eu–O4	128.77(15)	O4–Eu–N33	80.75(16)
O3–Eu–O4	129.15(15)	N43–Eu–N33	78.51(16)
O1–Eu–N43	140.01(15)	N23–Eu–N33	160.58(16)
O2–Eu–N43	77.16(16)	O1–Eu–N13	60.72(15)
O3–Eu–N43	88.45(16)	O2–Eu–N13	84.06(16)
O4–Eu–N43	62.06(15)	O3–Eu–N13	76.88(16)
O1–Eu–N23	85.69(16)	O4–Eu–N13	139.26(15)
O2–Eu–N23	136.02(16)	N43–Eu–N13	158.64(16)
O3–Eu–N23	61.22(16)	N23–Eu–N13	91.33(16)
O4–Eu–N23	80.07(16)	N33–Eu–N13	101.24(16)

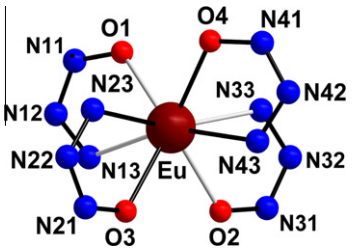

Fig. 2. Square antiprismatic structure of the core of the $P2_1/c$-type anion $[Eu\{O_2N(C_6H_4)NNN(O)Ph\}_4]^-$ (**2**). For clarity, the phenyl rings and the NO_2 groups, as well as the cation $[Et_3NH]^+$, the solvate molecule (H_2O), and the hydrogen atoms, are not shown.

3.2. HOMO–LUMO calculations, optical features and ground state structures

The HOMO–LUMO orbitals of the ligand 3-(4-nitrophenyl)-1-phenyltriazene N-oxide, as well as their energies, are shown in Table 4. The absorption spectra of the ligand are shown in Fig. 3, and both theoretical and experimental absorption spectra present the same profile. The utilization of DMSO as solvent has blocked the visualization of the bands in lower wavelengths. The theoretical and experimental ground state geometries for $[Eu\{O_2N(C_6H_4)NNN(O)Ph\}_4](Et_3NH)\cdot H_2O$ (**2**) are shown comparatively in Fig. 4. The average Eu–O/Eu–N distances obtained by monocrystal X-ray diffraction are 2.3337 and 2.5895 Å, respectively. With the Sparkle/AM1 program the average distances for Eu–O and Eu–N are 2.4303 and 2.5315 Å, respectively. For Eu–O the average error by the theoretical method is 4.1%, while for Eu–N the error is 2.2%. Although some differences regarding the coordination polyhedron are evident by the theoretical method, a good approximation with the structure obtained by X-ray diffraction was achieved.

Table 4
Ligand molecular orbital obtained by RM1.

Orbitals	Energy (eV)
HOMO	−3.8
LUMO	2.2

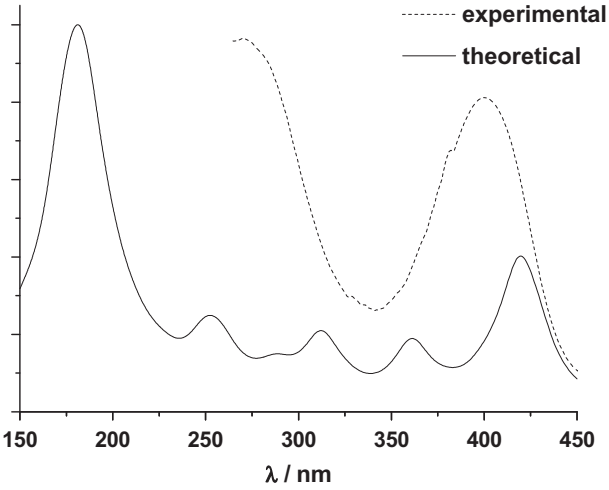

Fig. 3. Theoretical and experimental absorption spectra of the ligand.

3.3. Luminescence

As a first investigation, for determination of the triplet energy level of the ligand, the emission spectrum of the complex $[Gd\{O_2N-PhNNN(O)Ph\}_4](Et_3NH)\cdot H_2O$ was obtained (Fig. 5). The exceptionally high energy of the lowest excited level of Gd(III) affords an efficient method for this kind of measurement, after preparing the Gd(III) complex with the compound whose triplet energy is the point in question. The triplet energy is achieved through the centroid of the most intense transition, and for this (triazene-oxide) ligand, the triplet energy is located in 15086 cm^{-1}. The calculated triplet energy by INDO/S-CIS is 14921 cm^{-1}, a value very close to the experimental one. The energy levels diagram containing the theoretical and experimental energy levels for the ligand and Eu^{3+} is shown in Fig. 6. The triplet level of the ligand is situated below the emissor level of the europium ion. This circumstance makes the metal → ligand transfer rate more intense than the ligand → metal one. Thus, there is a competition between ligand emission through $T \rightarrow S_0$ transition and europium emission through $^5D_0 \rightarrow {}^7F_J$ ($J = 0, 1, 2, 3$ and 4) transitions. The europium emission is also affected by water molecules present in the complex structure. When the emission spectrum is performed at room temperature (~298 K) both ligand and europium emissions are observed. However, at low temperature there is a minimization of non-radiative deactivation processes caused by multi-phonon and multi-vibration due the presence of the water molecule. In this case, at ~77 K, the europium emission is predominant and the transitions $^5D_0 \rightarrow {}^7F_J$ ($J = 0, 1, 2, 3$ and 4) can be observed, as shown in Fig. 7. The occurrence of two bands in the $^5D_0 \rightarrow {}^7F_0$ region indicates the presence of two different and non-centrosymetric sites in the unit cell. These can be related to the Eu–O/Eu–N bonds, justifying the two bands for the $^5D_0 \rightarrow {}^7F_0$ transition. The high intensity of the hypersensitive $^5D_0 \rightarrow {}^7F_2$ transition reveals the high polarizability of the chemical environment around the europium ion, and the low split of the $^5D_0 \rightarrow {}^7F_2$ transition is a high symmetry indicative. $P2_1/c$ is one of the most symmetric space groups of the monoclinic

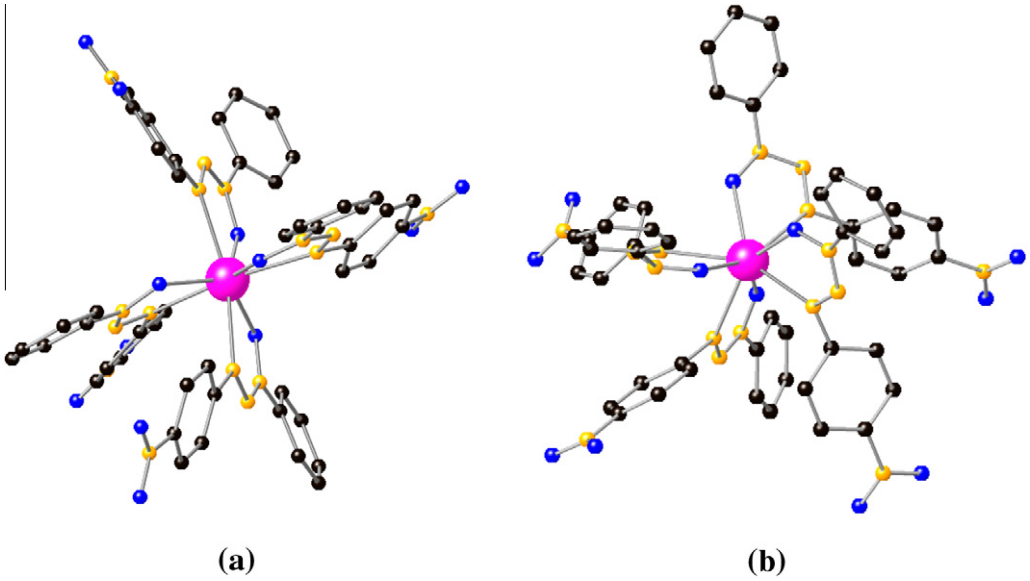

Fig. 4. Structure of the anion $[Eu\{O_2NPhNNN(O)Ph\}_4]^-$: (**a**) monocrystal X-ray diffraction; (b) sparkle/AM1.

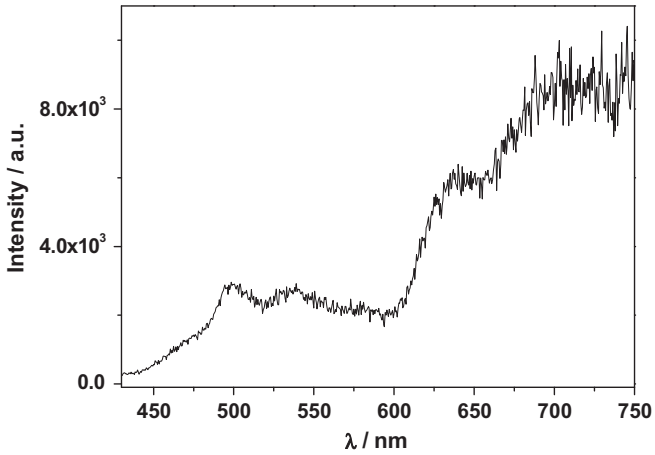

Fig. 5. Emission spectrum of the gadolinium compound, λ_{ex} = 420 nm.

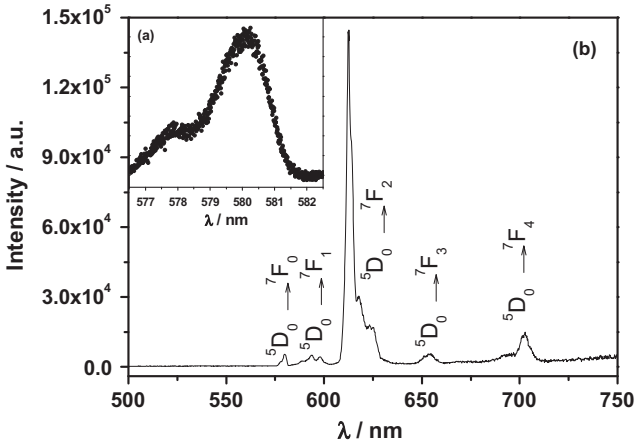

Fig. 7. Emission spectra of $[Eu\{O_2NPhNNN(O)Ph\}_4](Et_3NH)\cdot H_2O$ with λ_{ex} = 365 nm. (a) Enlargement of the $^5D_0 \rightarrow {}^7F_0$ transition; (b) full spectrum.

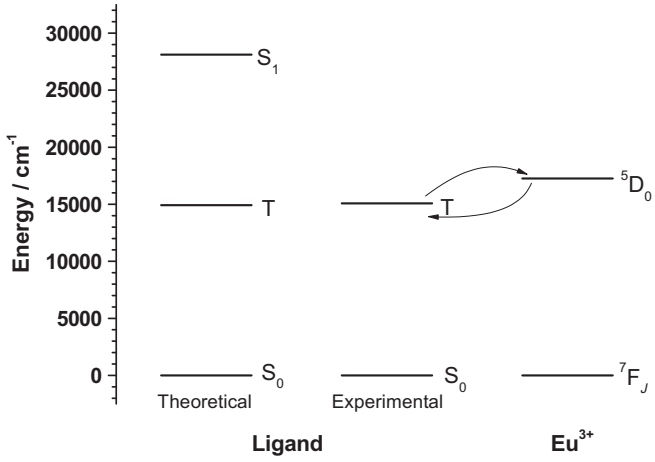

Fig. 6. Energy levels diagram for the ligand and europium(III).

system. As commented in the next section, luminescence experiments carried out with complexes **1**, **3** and **4** did not deliver mentionable results.

4. Conclusions

In the previous discussions we have shown that the chelate compounds $[Y^{III}\{O_2N(C_6H_4)NNN(O)Ph\}_4](Et_3NH)\cdot H_2O$ (**1**) and $[Ln^{III}\{O_2N(C_6H_4)NNN(O)Ph\}_4](Et_3NH)\cdot H_2O\cdot\{CH_3OH^*\}$ {Ln^{III} = Eu (**2**), Ho (**3**), Yb* (**4**)} are structurally equivalent, all of them retaining one water molecule as solvate. Yttrium resembles the lanthanides strongly in its chemistry, so that the triazene oxide complex of yttrium has been also included throughout this work. Although yttrium itself does not undergo luminescent transitions, its compounds are frequently useful host materials for later activators Ln^{3+} ions, like, for example, Eu:Y_2O_2S (standard material for the red phosphor in virtually all color and television cathode ray tubes) and Eu:Y_2O_3 (used for energy-efficient fluorescent tubes) [23].

Anhydrous salts of the lanthanides are known to exhibit luminescence which is exploited in their use as solid state laser materials or phosphors for color screens. By contrast, hydrated crystals of the lanthanides exhibit much lower luminescence intensity for the members in the center of the series (Sm, Eu, Gd, Tb, Dy), and essentially no luminescence at the beginning or end of the series [24]. The weak luminescence of hydrated Ln(III) ions

indicates that the high energy vibrations of the O–H groups of the water molecules embedded in the crystal lattice provide an efficient mechanism for the non-radiative de-excitation of the Ln(III) excited states. With basis on these statements, it is not surprising if only the Eu(III) complex presents luminescence, because Ho(III) and Yb(III) are situated at the end of the lanthanide series, and these complexes are also hydrated – in the case of Yb(III), with one additional methanol molecule. Some authors determine the number of H_2O molecules coordinated in the inner sphere of Ln(III) ions bound in complexes with basis on the luminescence lifetime of these hydrated complex ions. Haas and Stein [25] demonstrated that the observed luminescence decay constant for the $^5D_0$ excited state of Eu(III) in mixtures of water and acetonitrile is proportional to the number of water molecules in the primary coordination sphere of the ion. They also proposed that each water molecule quenches the excited state population independently.

Acknowledgments

This work was supported with funds from PRONEX-CNPq/FAPERGS (Brazil). J.H.S.K. Monteiro and M.R. Davolos acknowledge CAPES, CNPq and FAPESP (Brazil), as well as Prof. A.M. Simas for the valuable help in the computational techniques.

Appendix A. Supplementary material

CCDC 778915, 778914, 778913 and 779317 contains the supplementary crystallographic data for this paper. These data can be obtained free of charge from The Cambridge Crystallographic Data Centre via www.ccdc.cam.ac.uk/data_request/cif.

Supplementary data associated with this article can be found, in the online version, at doi:10.1016/j.ica.2010.11.007.

References

[1] M. Hörner, G. Manzoni de Oliveira, J.S. Bonini, H. Fenner, J. Organomet. Chem. 691 (2006) 655–658.
[2] M. Hörner, G. Manzoni de Oliveira, J.A. Naue, J. Daniels, J. Beck, J. Organomet. Chem. 691 (2006) 1051–1054.
[3] M. Hörner, G. Manzoni de Oliveira, M.B. Behm, H. Fenner, Z. Anorg. Allg. Chem. 632 (2006) 615–618.
[4] M. Hörner, G. Manzoni de Oliveira, L.C. Visentin, R.S. Cezar, Inorg. Chim. Acta 359 (2006) 4667–4671.
[5] M. Hörner, G. Manzoni de Oliveira, V.F. Giglio, L.C. Visentin, F. Broch, J. Beck, Inorg. Chim. Acta 359 (2006) 2309–2313.
[6] M. Hörner, G. Manzoni de Oliveira, L. Bresolin, A.B. de Oliveira, Inorg. Chim. Acta 359 (2006) 4631–4634.
[7] M. Hörner, G. Manzoni de Oliveira, E.G. Koehler, L.C. Visentin, J. Organomet. Chem. 691 (2006) 1311–1314.
[8] M. Hörner, G. Manzoni de Oliveira, A.J.R.W.A. Santos, Z. Anorg. Allg. Chem. 633 (2007) 971–973.
[9] M. Elkins, L. Hunter, J. Chem. Soc. 4 (1940) 653–655.
[10] M. Hörner, B.A. Iglesias, P.R. Martins, P.C.M. Villis, L.C. Visentin, Z. Anorg. Allg. Chem. 634 (2008) 1058.
[11] M. Hörner, B.A. Iglesias, P.R. Martins, P.C.M. Villis, Anal. Sci.: X-ray Struct. Anal. Online 24 (2008) x123.
[12] G. Manzoni de Oliveira, M. Hörner, A. Machado, M.A. Villetti, D.F. Back, B.A. Iglesias, J. Mol. Struct. 928 (2009) 85–88.
[13] G. Gasparotto, M.A. Cebim, M.S. Goes, S.A.M. Lima, M.R. Davolos, J.A. Varela, C.O. Paiva-Santos, M.A. Zaghete, J. Appl. Phys. 106 (2009) 063509.
[14] K. Binnemans, Chem. Rev. 109 (2009) 4283.
[15] G.M. Sheldrick, Acta Crystallogr., Sect. A 64 (2008) 112.
[16] G.B. Rocha, R.O. Freire, A.M. Simas, J.J.P. Stewart, J. Comput. Chem. 27 (2006) 1101.
[17] J.J.P. Stewart, MOPAC2009 Manual; Colorado Springs, Stewart Computational Chemistry, 2009.
[18] R.O. Freire, G.B. Rocha, A.M. Simas, Inorg. Chem. 44 (2005) 3299.
[19] J.E. Ridley, M.C. Zerner, Theor. Chim. Acta 42 (1976) 223.
[20] M.C. Zerner, G.H. Loew, R.F. Kirchner, U.T. Mueller-Westerhoff, J. Am. Chem. Soc. 102 (1980) 589.
[21] M.C. Zerner, ZINDO Manual; Quantum Theory Project, University of Florida, Gainesville, FL, 1990.
[22] A. Bondi, J. Phys. Chem. 68 (1964) 441.
[23] S. Cotton, Lanthanide and Actinide Chemistry, John Wiley and Sons, Ltd., West Sussex, England, 2006. p. 114.
[24] G.R. Choppin, D.R. Peterman, Coord. Chem. Rev. 174 (1998) 283.
[25] Y. Haas, G. Stein, J. Phys. Chem. 75 (1971) 3677.